Journal of Photochemistry and Photobiology A: Chemistry 201 (2009) 15–22

Contents lists available at ScienceDirect

Journal of Photochemistry and Photobiology A: Chemistry

journal homepage: www.elsevier.com/locate/jphotochem

Photocatalytic decomposition of 4-chlorophenol over an efficient N-doped TiO_2 under sunlight irradiation

Hongqi Sun, Yuan Bai, Huijing Liu, Wanqin Jin*, Nanping Xu

State Key Laboratory of Materials-Oriented Chemical Engineering, College of Chemistry and Chemical Engineering, Nanjing University of Technology, Nanjing 210009, PR China

ARTICLE INFO

Article history:
Received 29 January 2008
Received in revised form 10 June 2008
Accepted 22 August 2008
Available online 26 September 2008

Keywords:
TiO_2
Nitrogen-doped
Photocatalyst
Visible light

ABSTRACT

Using a new nitrogen precursor of a mixture of ammonia and hydrazine hydrate, N-doped TiO_2 photocatalyst with a high efficiency under visible light was synthesized by a precipitation method. The analysis of X-ray photoelectron spectroscopy (XPS) suggested that the doping concentration of nitrogen was 0.45 at%, while it was 0.21 at% or 0.24 at% using single ammonia or hydrazine hydrate as nitrogen precursor. The patterns of the electron paramagnetic resonance spectroscopy (EPR) indicated that the paramagnetic species of NO_2^{2-}, NO and Ti^{3+} existed as the proposed active species. The ultraviolet–visible (UV–vis) spectra revealed that the band-gap of the N-doped TiO_2 was 3.12 eV, which was slightly lower than 3.15 eV of pure TiO_2. The N-doped TiO_2 showed higher efficiency under both ultraviolet (UV) and visible light irradiations. Moreover, the degradation grade of 4-chlorophenol (4-CP) using the as-synthesized N-doped TiO_2 under sunlight irradiation for 6 h was 82.0%, which was higher than 66.2% of the pure TiO_2, 60.1% or 65.2% of the N-doped TiO_2 using single ammonia or hydrazine hydrate as precursor. Density functional theory (DFT) calculations were performed to investigate the visible light response of the N-doped TiO_2. Our study demonstrated that the visible activities vary well with the concentrations of NO_2^{2-} species incorporated by N–TiO_2 series photocatalysts and the higher activity of the as-prepared N-doped TiO_2 was attributed to the enhancement of the concentration of NO_2^{2-} species.

1. Introduction

As an alternative way to the conventional methods, photocatalysis has been widely used in energy conversion, air purification, and organic contaminant mineralization [1,2]. Solar energy is clean, renewable, and abundant, so using solar energy to execute photocatalysis processes has become a dream of researchers for several decades. The energy of visible fraction is about 42% of solar spectra compared with the ultraviolet (UV) less than 5%. So, many efforts have been devoted to the visible response of photocatalysts [3–8]. Titanium dioxide (TiO_2) has attracted extensive interest because of its high activity, low cost, and long-time stability. However, it can be activated only in the small UV fraction (<400 nm) due to its large band-gap of about 3.2 eV. To utilize solar energy efficiently, much attention has been directed toward the development of nonmetalion doped TiO_2 [9–13]. Among these studies, the nitrogen-doped TiO_2 photocatalysts have become the hottest topic in the field of visible photocatalysis.

The photocatalytic activity of nitrogen-doped TiO_2 under visible light irradiation is highly depended on the chemical compositions of the dopants, which are directly determined by the preparation conditions as well as the nitrogen precursors. Several studies indicated that the substitutional nitrogen doping (formation of Ti–N bond) would come from the following conditions: (i) calcination of TiO_2 or $Ti(OH)_4$ at about 550 °C under NH_3 or NH_3/Ar atmosphere [4], (ii) oxidation of TiN [14], (iii) sputtering the TiO_2 target in an N_2/Ar gas [4,15,16] and (iv) atmospheric microwave plasma-torch using gas-phase $TiCl_4$ [17], etc. Mild preparation conditions (calcination temperature lower than 400 °C) would induce the formation of NO_x as the dopants of N–TiO_2: (i) annealing the precipitation of hydrolysis of Ti-precursor with addition of NH_4OH [9], $(NH_4)_2CO_3$ or NH_4HCO_3 [18] and (ii) using organic compounds urea [19], thiourea [20], guanidine [19] or triethylamine [21] as nitrogen precursors. Above studies suggested that the nitrogen precursors play a key role in preparation of nitrogen-doped TiO_2. Li et al. [19] and Nosaka et al. [22] studied the effects of nitrogen precursors on visible activity of nitrogen-doped TiO_2. However, most of these precursors varied in the region of organic compounds with the same chemical states. Accordingly, it is important to evaluate the effects of inorganic nitrogen precursors with different chemical states on the physiochemical properties and photocatalytic activity of NO_x-doped TiO_2.

In our previous work [23], we synthesized a visible light active TiO_2-doped with low concentration of NO_x using hydrazine hydrate

* Corresponding author. Tel.: +86 25 83587211; fax: +86 25 8358 7211.
E-mail address: wqjin@njut.edu.cn (W. Jin).

1010-6030/$ – see front matter © 2008 Elsevier B.V. All rights reserved.
doi:10.1016/j.jphotochem.2008.08.021

as a precursor and found that it was of higher activity under both UV and visible irradiations. However, our further study showed that its activity under natural sunlight was still not acceptable. The activity of nitrogen-doped TiO_2 under sunlight needs further improvement. In this work, therefore, the N-doped TiO_2 was synthesized using the mixture of ammonia and hydrazine hydrate as precursors. Higher efficiencies of the N-doped TiO_2 were obtained under visible as well as sunlight irradiations than that derived from single ammonia or hydrazine hydrate. The crystal structures, optical properties, doping species and photocatalytic activities under various irradiation conditions (UV, visible and sunlight) of the N–TiO_2 series were studied in detail.

2. Experimental

2.1. Catalysts preparation

The N-doped TiO_2 was synthesized by hydrolyzing $TiCl_4$ with addition of nitrogen precursor. $TiCl_4$ of 0.05 mol was added dropwise into pure water of 400-mL while it was surrounded by an ice bath. After stirring for several minutes, a 5 mol/L mixed solution of ammonia and hydrazine hydrate was added dropwise to adjust the pH value to 5.5. The obtained precipitation was filtered and washed by water for several times after aging for 24 h. The precipitation was first dried at 343 K in air to remove water, then calcinated at 673 K for 4 h to obtain the nitrogen-doped TiO_2 photocatalysts. Other N-doped TiO_2 series were synthesized by the same procedures. The catalysts derived from ammonia, hydrazine hydrate and their mixture were denoted as TN1, TN2, and TN3, respectively. Pure TiO_2 was obtained from the same procedure by addition of sodium hydroxide instead of nitrogen donors.

2.2. Characterization

The X-ray diffraction (XRD) patterns were obtained on a Bruker D8-Advance X-ray diffractometer using a Cu target Kα radiation (λ = 1.5405 Å) to determine the crystalline phase. The XRD patterns of (1 0 1) plane was at the scanning range 2θ 24.0–26.5° with the scanning rate of 0.02° s^{-1}. The Brunauer–Emmett–Teller (BET) surface area and pore size distribution were evaluated using a Quantachrom Chemeet-300 nitrogen adsorption apparatus. The states of the charges were investigated by X-ray photoelectron spectroscopy (XPS) using an ESCALab MK2 instrument with a Mg X-ray source. The paramagnetic species of nitrogen and Ti^{3+} in the as-synthesized nitrogen-doped TiO_2 photocatalysts were measured on an electron paramagnetic resonance spectroscopy (EPR) using a Bruker EMX-10/12 instrument. The UV–vis reflectance spectra (UV–vis) were recorded with a Shimadzu UV-2401TC UV–vis spectrophotometer, using $BaSO_4$ as reference. The concentration of 4-chlorophenol was determined by measuring the decrease of the absorbance at 225 nm on a Lambda 35 UV–vis spectrophotometer. The total organic carbon (TOC) was analyzed using a Shimadzu TOC-VCPH analyzer to evaluate the photomineralization degree of 4-chlorophenol (4-CP).

2.3. Evaluation of the photocatalytic activity

Photodegradation experiments were carried out with 100 mg sample of powders suspended in 100 mL of a 4-CP solution in a 250 mL reactor. A recycling water jacket was used to keep the reactor temperature constant at 30 ± 0.2 °C. A 250 W Xe lamp was used as the visible light source, which irradiated outside (at a distance of 15 cm from the solution surface) through a 400 nm cutoff filter onto the reactor. Experiments on the photocatalytic degradation of 4-CP under UV irradiation were conducted by the same method without the cutoff filter and with a 250 W high-pressure mercury lamp as the UV source. The reaction systems were magnetic stirred all the time. The irradiance intensities of Vis of Xe lamp and UV of mercury lamp were 40.9 and 480.0 μW/cm^2, respectively. Photocatalytic experiments under sunlight irradiation were carried out with 200 mg catalyst suspended in 200 mL of 4-CP solution in a 250 mL conical flask.

3. Results and discussion

3.1. Crystal structure and microstructure analysis

Fig. 1 shows the XRD patterns of the samples, indicating that all the samples are dominating of anatase phases. The pure TiO_2 consists of 96.2% of anatase and 3.8% of brookite phase content. The anatase phase contents of samples TN1–3 are 99.3%, 89.7%, and 92.9%, respectively. The average crystalline sizes were calculated using the Scherrer's formula: $D = K\lambda/\beta\cos\theta$. The crystal sizes of pure TiO_2, TN1, TN2, and TN3 are 9.5, 12.2, 12.2, and 12.0 nm, respectively. The inset of Fig. 1 shows the shifts of (1 0 1) peaks of the nitrogen-doped titania, compared with the pure TiO_2. No obvious shifts of TN1 and TN2 were found, while the (1 0 1) peak of TN3 shift significantly to higher 2θ degree of about 0.10°. The shift indicates that the crystal of TN3 is distorted by the incorporation of nitrogen and contains internal strain [7,24–26].

Fig. 2 displays the curve of the pore size distribution and the inset shows the corresponding nitrogen adsorption–desorption isotherms of TN3. An IV-type N_2 isotherm with hysteresis loops indicates that the sample is of the mesoporous nature. There is a diffusion bottleneck, which is possibly caused by the nonuniform pore size [12]. An obvious hysteresis loop locates at the high relative pressure region, which shows the capillary condensation is associated with large pore channels [27]. The specific surface area of TN3 calculated from the BET plot is 96.7 m^2/g, and the pore size distribution calculated from the desorption branch of the nitrogen isotherm shows a narrow range of 3.0–11.0 nm with an average pore diameter of 10.6 nm and a pore volume of 0.2623 cm^3/g.

Fig. 2 curve of pore size distribution calculated from the desorption branch of the nitrogen isotherm by the BJH method and the corresponding nitrogen adsorption–desorption isotherms (inset) of TN3.

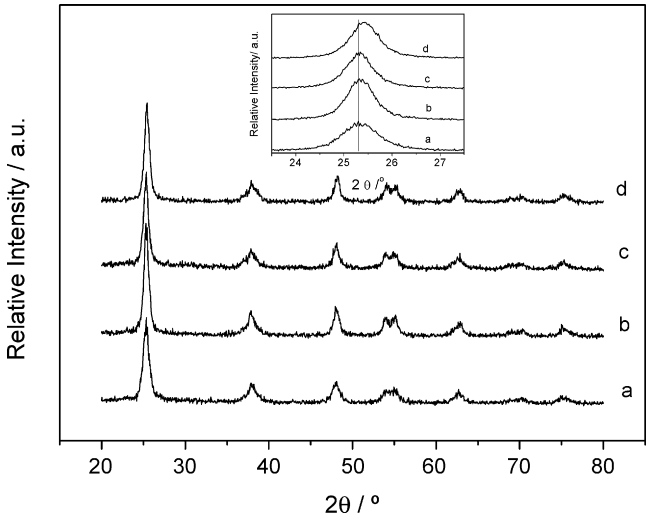

Fig. 1. XRD patterns of various samples; inset: XRD patterns on (1 0 1) planes of various samples. (a) TiO_2; (b) TN1; (c) TN2; (d) TN3, $N_2H_4{\cdot}H_2O$:$NH_4{\cdot}OH$ = 1:1.04 (mol).

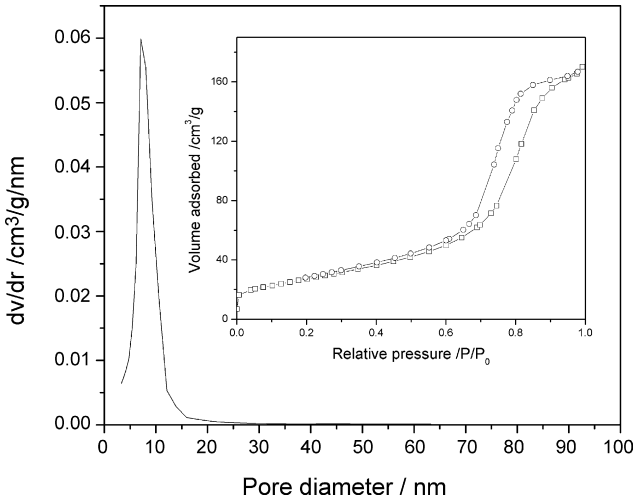

Fig. 2. Curve of pore size distribution calculated from the desorption branch of the nitrogen isotherm by the BJH method and the corresponding nitrogen adsorption–desorption isotherms (inset) of TN3.

3.2. Chemical composition of the N-doped TiO_2

To investigate the chemical states of the doping nitrogen species, XPS spectra were applied to examine three areas. Fig. 3(A) shows N 1s spectra of the three nitrogen-doped samples. The doping nitrogen concentrations of samples TN1–3 are 0.21, 0.24, and 0.45 at%, respectively. No obvious signals at about 396 eV were found, while the peaks in the region of 396–400 eV might indicate that little amount of nitrogen atoms form Ti–N bonds in the crystal of TiO_2 [4,14,15,17]. As shown, the obvious peaks of all three samples are centered at about 400 eV seems, which is important for the visible response. The peaks at the range of 399–401.5 eV arise from the presence of NO [21,23]. Several researchers [21,28–30] had ever suggested that the N-doped TiO_2 contained a series N-containing species, e.g., NO, NO_2, NO^{2-} and $NO_2{}^{2-}$, etc. The splitting or shift of the NO signal at the range of 399–401.5 eV possibly suggests the presence of different N electron densities via different interaction types of NO with TiO_2, which was also confirmed by the following EPR spectra. However, those N-containing species, such as molecular NO_2, which have too large radii to dope into TiO_2 crystal, so they can only exist at the surface of the catalysts particles or be adsorbed

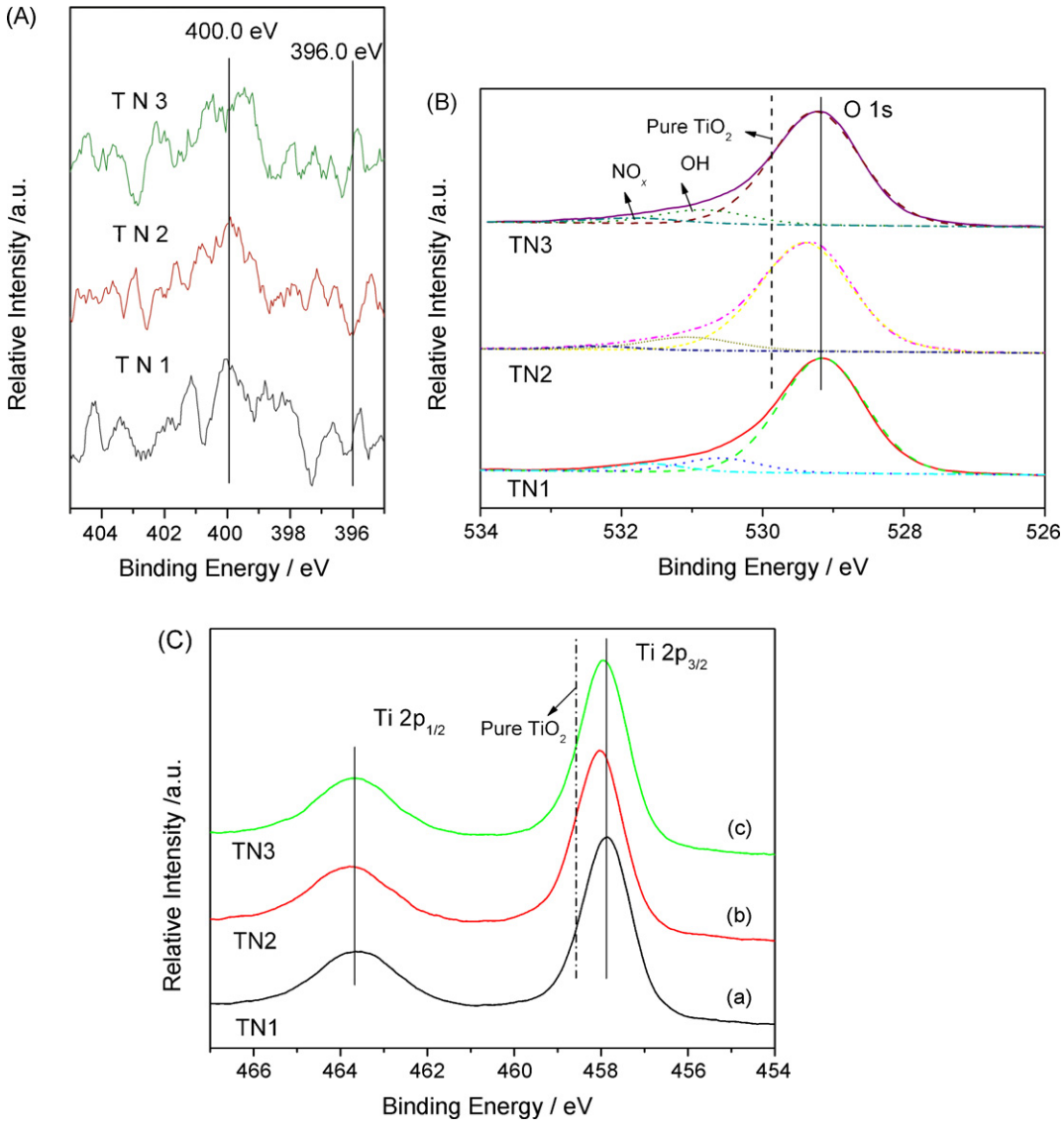

Fig. 3. N 1s (A), O 1s (B), Ti 2p (C), and XPS spectra of various N-doped TiO_2.

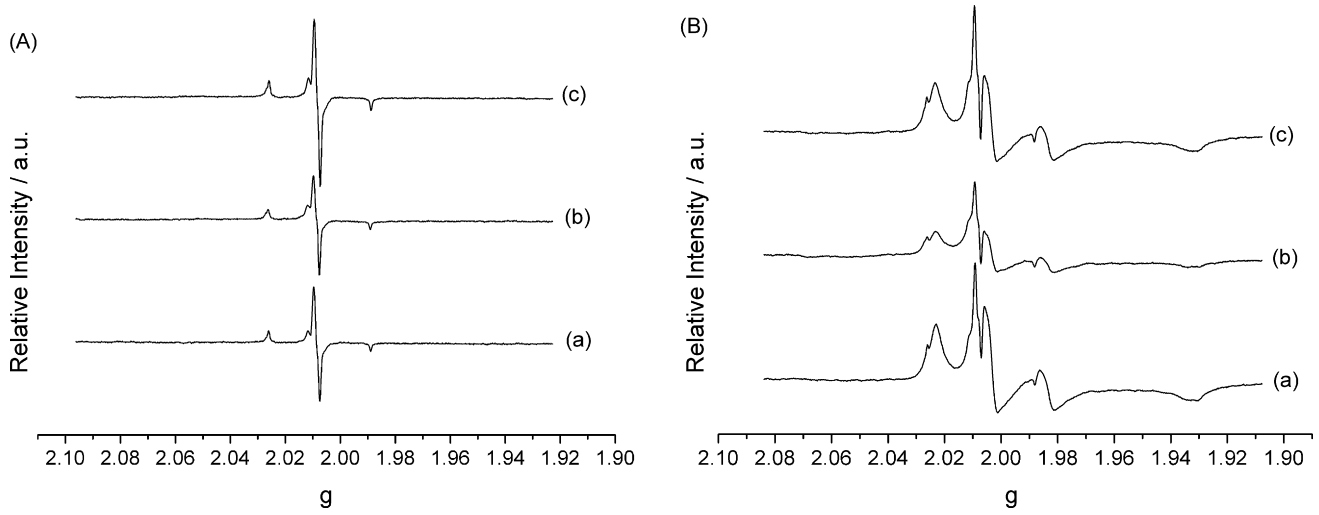

Fig. 4. EPR spectra of (a) TN1, (b) TN2, and (c) TN3, measured at (A) ambient temperature and (B) 110 K.

at the mesopores and not influence the electronic structure of the solid [31].

Fig. 3(B) displays XPS O 1s spectra. Through de-convolution based on the profile of O 1s, three peaks are found at about 529.3, 530.9 and 531.9 eV in TN3. The first peak can be assigned to the lattice oxygen of TiO_2, the second peak arises from OH radical, and the last peak can be contributed to the presence of the oxygen of NO_x. The peak of O 1s spectrum of the oxygen in pure TiO_2 crystal is at 529.9 eV, while the peaks of TN1, TN2, and TN3 are found to shift to lower binding energy about 0.7, 0.5, and 0.6 eV, respectively. These shifts indicate an increase in the electron densities of the O atoms.

The XPS spectra of Ti 2p region are shown in Fig. 3(C). The XPS spectra of Ti 2p3/2 of TN3 can be fitted as one peak at 457.9 eV. The XPS Ti 2p3/2 spectrum of pure TiO_2 is at 458.6 eV, whereas the spectra of XPS Ti 2p3/2 spectra of TN1, TN2 and TN3 shift to lower binding energies of 0.7, 0.6, and 0.7 eV, respectively, indicating the increase of the electron densities of the Ti atoms. This suggests that some Ti^{3+} species exist in the three samples [32].

The paramagnetic species in the impure semiconductor catalysts were detected by EPR spectra. Fig. 4 shows that the paramagnetic species of nitrogen and Ti^{3+} are present in the as-synthesized TiO_2-based photocatalysts. At ambient temperature, g tensors at 2.0261, 2.0083 and 1.9881 were found in TN3, as shown in Fig. 4(A). Sakatani et al. reported that three peaks at $g = 2.022$, 2.004, and 1.983 were found in the nitrogen-doped TiO_2 using EPR at 77 K [29]. These signals arise from the presence of NO_2^{2-}, which can be regarded as the interaction between NO with the surface O^{2-}. For TN1, these signals can be found at $g = 2.0260$, 2.0083 and 1.9981, and $g = 2.0261$, 2.0083 and 1.9881 for TN2, respectively. In all analysis of the samples, the same amounts of catalysts (150 mg) were used to compare the signal intensities of the three samples quantitatively. The relative intensities of the g tensors indicate the amounts of NO_2^{2-} species in the samples. Therefore, the amounts of NO_2^{2-} species in the samples were in the order of TN3 > TN1 > TN2. With decreasing the temperature to 77 K, these signals were buried in the other more intense signals of N-containing species which were proven to be NO [33]. Different from the results of Livraghi et al. [33], when we decreased the temperature to 110 K, the NO_2^{2-} signals still existed ($g = 2.020$, 2.0084, and 1.9888). Moreover, some other new signals appeared, as shown in Fig. 4(B). Three g tensors at 2.0231, 2.0034 and 1.9812 were found in EPR spectra, indicating the presence of NO in the as-prepared powders. Furthermore, the hyperfine structures in the EPR spectra of the N-doped TiO_2 further confirmed the presence of NO. The hyperfine splitting was at the region from 1.9339 to 1.9309, 1.9345 to 1.9295, and 1.9335 to 1.9305 for TN1, TN2 and TN3, respectively. The amounts of NO in the catalysts were in the order of TN1 > TN3 > TN2.

3.3. The UV–vis spectroscopy

The optical properties of the as-synthesized samples were investigated by the UV–vis spectroscopy, as shown in Fig. 5. The band-gap of TiO_2 can be estimated from the intercept of UV–vis spectra using the following equation: $E_g = 1240/\lambda$ [15,23,34]. The absorption threshold of pure TiO_2 is 393.7 nm, which is corresponding to a band-gap of 3.15 eV. It cannot respond to visible light. When the N-containing species were incorporated into TiO_2, the catalysts showed a color of pale yellow. The band-gap energies of samples TN1–3 are 3.08, 3.14 and 3.12 eV, respectively. The minor narrowing of the band-gap of TN series (~0.02 eV) compared to pure TiO_2 might be attributed to the presence of trace amount Ti–N bonds or Ti^{3+} species. A new absorption region started at 550 nm (2.25 eV) after nitrogen doping. As suggested by Lindgren et al. [35], the new spectral band in the range $397 < \lambda < 550$ nm was not from a band-to-band transition but from excitation of electrons from local states in the band-gap to unoccupied states. Combining the UV–vis analysis

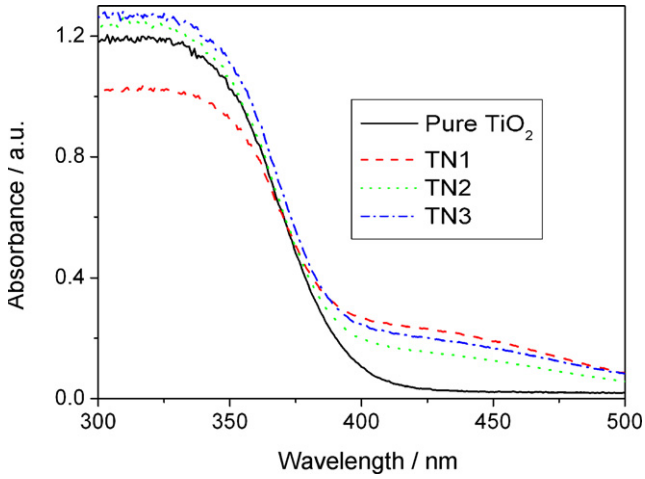

Fig. 5. The UV–vis diffusive adsorption spectra of various photocatalysts.

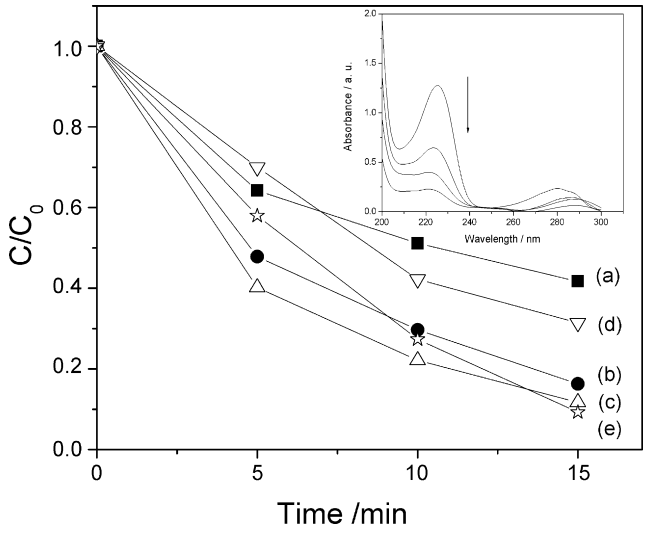

Fig. 6. Efficiency of photodegradation of 4-CP (1.5×10^{-4} M) in the presence of various photocatalysts (1 g/L) under UV: (a) TiO_2; (b) TN1; (c) TN2; (d) TN3; (e) P25.

with the EPR observation, it can be deduced that the NO species can interact with the surface oxygen of the semiconductor without electron transfer to metal and then remain as NO_2^{2-} species, therefore the manifold of surface states must exist [15,20]. The presence of surface states would be the origin of the visible activity of these nitrogen-doped TiO_2 catalysts. Although other NO_x species even affect the optical property of TiO_2, they would not contribute to visible photocatalysis [23,31].

3.4. Photocatalytic activities of the as-synthesized catalysts

The activities of the as-synthesized photocatalysts were evaluated by measuring the degradation efficiencies of 4-CP (1.5×10^{-4} mol L^{-1}) under UV, visible and sunlight (direct/indirect) irradiations, respectively.

3.4.1. Photocatalysis under UV irradiation

Fig. 6 shows the efficiencies of photodegradation of 4-CP under UV in the presence of various photocatalysts. A commercial available photocatalyst of Degussa P25 was used as a reference photocatalyst. The apparent-reaction-rate constants of TiO_2, TN1, TN2, TN3, and P25 are 0.0667, 0.1302, 0.1631, 0.07931, and 0.1428 min^{-1}, respectively. All the nitrogen-doped TiO_2 showed higher activities than that of pure TiO_2. Among the nitrogen-doped TiO_2, TN3 was of lower activity than both of those of TN1 and TN2 under UV irradiation, which would be attributed to the higher impurity concentration. Typical UV–vis absorption spectra of 4-CP dependent on the degradation time were recorded as action spectra. The inset in Fig. 6 is the action spectra of degradation of 4-CP using TN3 under UV.

3.4.2. Photocatalysis under visible irradiation

Fig. 7 shows the photocatalytic activities of various catalysts under visible irradiation. The pure TiO_2 has no activity under visible irradiation. The nitrogen-doped TiO_2 could efficiently degradation of 4-CP. The apparent-reaction-rate constants of TN1, TN2, and TN3 are 0.00199, 0.00185, and 0.00232 min^{-1}, respectively. TN1 and TN2 had comparable activity under visible, and the activity of TN3 was higher than those of others. The inset in Fig. 7 is the action spectra of degradation of 4-CP using TN3 under visible irradiation. It shows that the concentrations of 4-CP decrease regularly with the degradation time. It is well known that one of the most attractive

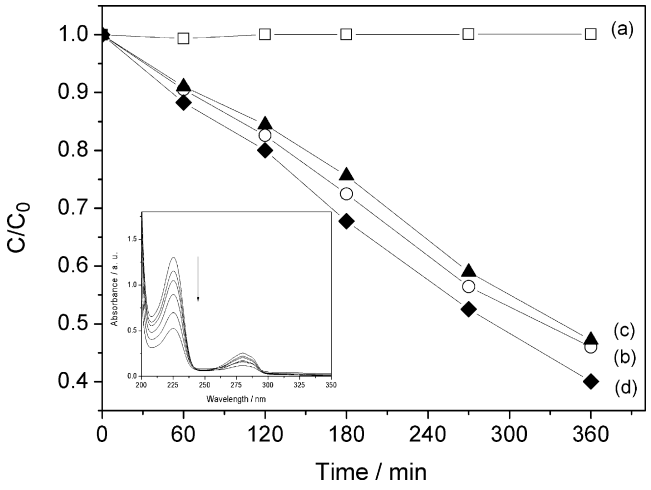

Fig. 7. Efficiency of photodegradation of 4-CP under visible irradiation: (a) TiO_2; (b) TN1; (c) TN2; (d) TN3.

reasons for using photocatalysis technology to purify water is that the organic pollution can be decomposed completely to H_2O, CO_2 and other inorganic ions [8,23]. So, TOC analysis were applied to detect the mineralization grades of the as-decomposed 4-CP under visible irradiation. Fig. 8 shows the efficiencies of photomineralization of 4-CP using various catalysts under visible irradiation. The results further confirmed that TN3, derived from the mixture of hydrazine hydrate and ammonia, has the highest activity among TN1, TN2 and TN3 under visible light irradiation.

3.4.3. Photocatalysis under sunlight irradiation

Using solar energy to execute water purification processes is the direction of the scientific research on photocatalysis. Fig. 9 shows the efficiency of degrading 4-CP under sunlight irradiation. In the first 3 h, the reaction system was exposed directly under sunlight, and then the system was irradiated by diffusive sunlight for 3 h. In the first 90 min, the concentration of 4-CP photodegraded using pure TiO_2 decreased slightly, while the mixed solution had turned from milk-white to the color of pale red (started at about 15 min) during this process. This is because some development dyes, e.g., quinone or hydroquinone, were produced as intermediates when chlorophenol was photodegraded under UV [36,37]. These species could be activated by visible light to generate elec-

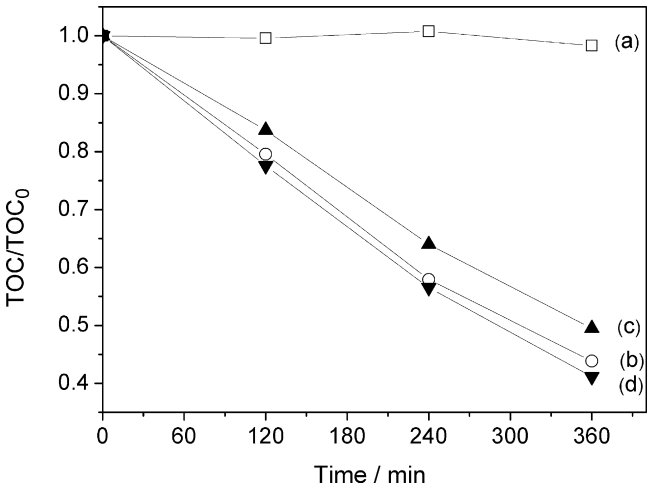

Fig. 8. Photomineralization of 4-CP under visible irradiation: (a) TiO_2; (b) TN1; (c) TN2; (d) TN3.

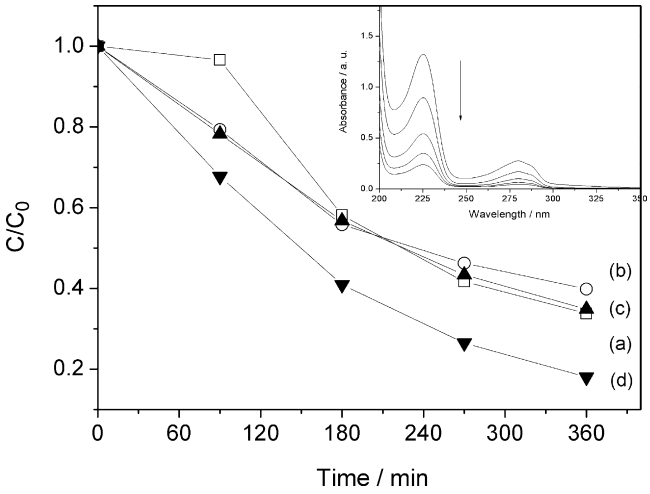

Fig. 9. Efficiency of photodegradation of 4-CP under solar-light: (a) TiO_2; (b) TN1; (c) TN2; (d) TN3.

trons, then these electrons were transferred to the conduction band of TiO_2 to carry out photocatalysis reactions. Then, the concentration of 4-CP decreased rapidly. Those reaction systems using TN series maintained the color of solution constant throughout the photocatalysis processes, although intermediates would also be produced [8]. After degradation time reached 180 min, the degradation degrees of 4-CP using pure TiO_2 and TN1–3 were 41.9, 44.2, 43.26 and 59.1%, respectively. The activity of TN1 or TN2 was just somewhat higher than that of pure TiO_2 under direct sunlight irradiation in former 3 h. Otherwise, TN3 showed the highest activity among all the catalysts including pure TiO_2. In later 3 h, all systems were under diffuse sunlight irradiation, and ultimately, the degradation degrees of 4-CP using pure TiO_2 and TN1–3 were 66.2, 60.1, 65.2 and 82.0%, respectively. TN3 also showed superior activity than other as-prepared photocatalysts. The inset of Fig. 9 is the action spectra of 4-CP using TN3 for photocatalysis. The TOC values of the as-degraded 4-CP were detected, as shown in Fig. 10. The comparison of the activities of pure TiO_2, TN1, and TN2 with the results of Fig. 9 show minor difference, but the photomineralization efficiency of TN3 is still the highest. The irradiance intensities of UV and visible in sunlight were recorded, as shown in the inset of Fig. 10.

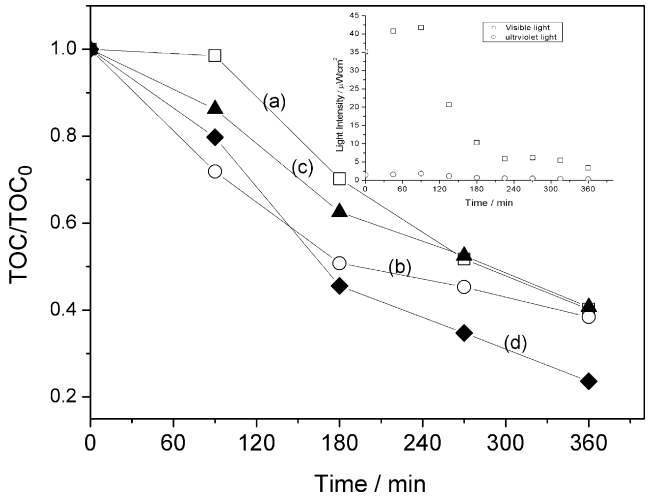

Fig. 10. Photomineralization of 4-CP under solar light: (a) TiO_2; (b) TN1; (c) TN2; (d) TN3; inset: irradiance intensities depend on time.

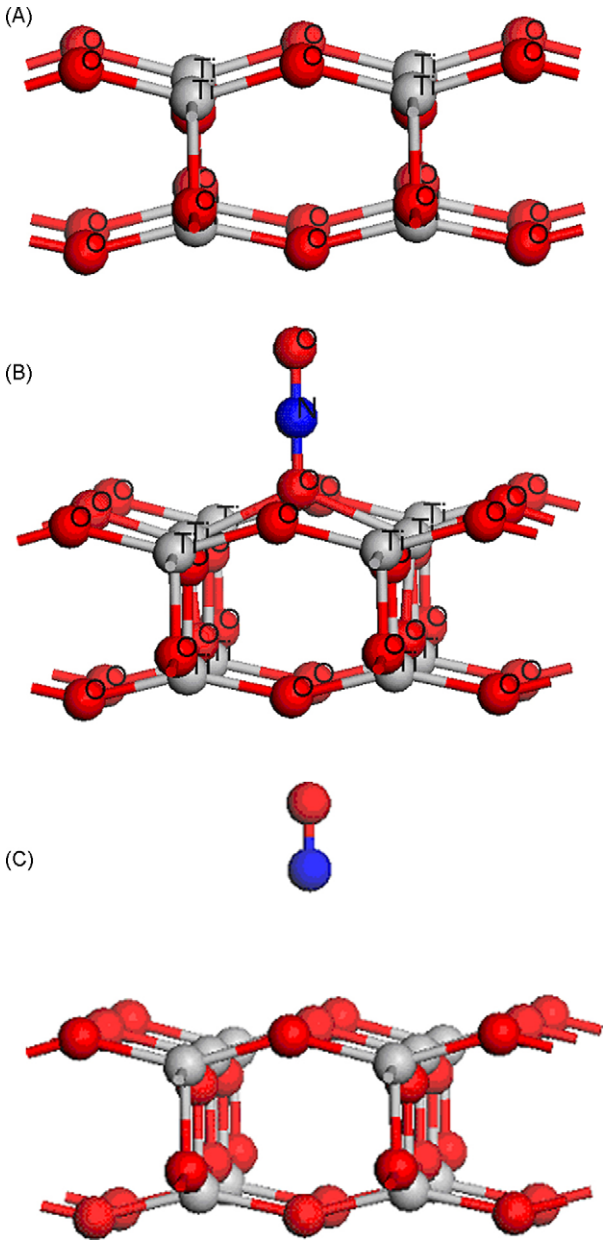

Fig. 11. Surface structure models of: (A) anatase TiO_2 (2 × 2) (0 0 1) surface; (B) NO_2^{2-} in the surface; (C) NO in the surface.

Photocatalysis experiments showed that TN3 derived from the mixed solutions is of the highest activity under both visible and sunlight irradiations among TN series. Because the visible activity is attributed to nitrogen doping, the concentration varieties of N-containing species would induce the higher visible activity of TN3. Previously analysis of XPS and EPR revealed that the concentrations of total nitrogen, NO, and NO_2^{2-} were in the order of TN3 > TN2 > TN1, TN1 > TN3 > TN2, and TN3 > TN1 > TN2, respectively. It is found that the concentration of NO_2^{2-} is according well with the visible activities of TN3 > TN1 > TN2. As mentioned above, in low concentration nitrogen-doped TiO_2, especially the effective impurity was NO_x, the visible activity was not due to band-gap narrowing but due to the formation of surface states [23,31]. So, the higher visible activity of TN3 was then attributed to the higher concentration of NO_2^{2-} derived from the mixed solution of ammonia and hydrazine hydrate.

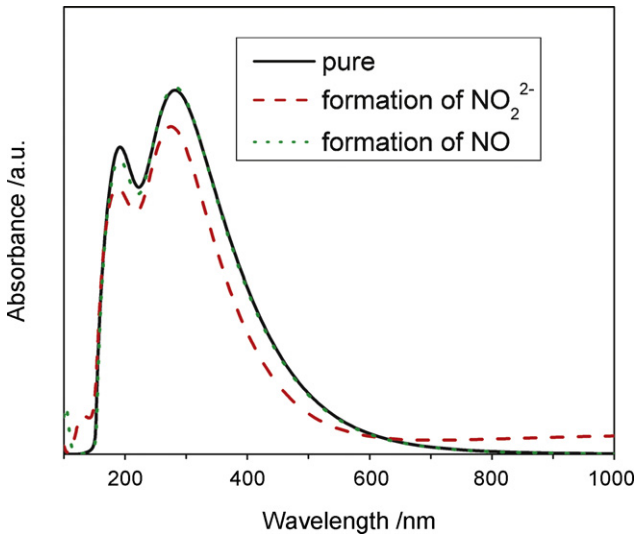

Fig. 12. The optical properties of different models obtained by DFT calculations.

3.5. The mechanism of visible light response of N-doped TiO_2

XPS studies showed that the N-containing impurities are series NO_x species with trace substitutional N atoms. EPR spectra further confirmed that the paramagnetic species of both NO and NO_2^{2-} are present in the doped samples. The experiments of photodegradation of 4-CP suggested that NO_2^{2-} would be active species for visible light sensitivity. The mechanism of visible response of substitutional N-doped TiO_2 has also been studied using density functional theory (DFT) by many researchers [4,14,38,39], however, few studies have mentioned on NO_x-doped TiO_2. Valentin and coworkers [40], and Sanz and coworkers [41] had studied on nitrogen doping at the anatase TiO_2 (1 0 1) and rutile TiO_2 (1 1 0), respectively. Otherwise, those models did not cover the species of NO and NO_2^{2-}. Therefore, we established an anatase TiO_2 (2×2) (0 0 1) surface to describe the NO or NO_2^{2-} doping, which were observed by XPS and EPR spectra. NO binding to surface O^{2-} was used to simulate the formation of NO_2^{2-}, isolate NO molecular in the vacuum slab was used to define the NO. These models were shown in Fig. 11. The electronic band structures and optical properties were investigated by DFT calculations [42]. The methodology was checked by calculation of the cell parameters and band-gap energy of bulk anatase TiO_2, which are $a = b = 3.785$, $c = 9.814$, $E_g = 2.07$ eV, comparing to experimental data $a = b = 3.780$, $c = 9.514$, $E_g = 3.20$ eV. In our work, the band-gap is comparable to the datum in literature [43] but still largely underestimated compared with experimental, due to the well-known shortcoming of GGA.

The calculated band structures showed that the band-gap energies of anatase TiO_2 (2×2) (0 0 1) surface, NO_2^{2-} doping and NO doping are 1.79, 2.03 and 1.80 eV, respectively. It is clearly showed that the species NO_2^{2-} is not contributed to the band-gap narrowing like the contribution of substitutional N doping, while somewhat enhances the band-gap energy. As to NO, a typical NO_x, it would not influence the electronic structures of the solid. The results of DFT calculations are consistent well with the experimental and other studies [31,33]. Fig. 12 displays the calculated optical properties of related models. It further shows that the NO would slightly change the optical property of TiO_2 when absorption wavelength is larger than 200 nm. A new absorption band appears in visible light region with the formation of NO_2^{2-}, which is consistent with the UV–vis spectra showed previously. The new absorption band arises from the energy levels which are at a distance of 0.38 eV from the bottom of conduction band.

4. Conclusions

N-doped TiO_2 with a high efficiency under visible light irradiation was synthesized using a mixed solution of ammonia and hydrazine hydrate as nitrogen precursors. The visible and sunlight photocatalytic activity of this catalyst was higher than those using single ammonia or hydrazine hydrate. XPS analysis showed that the nitrogen donors controlled the concentration and the kind of the impurities, which could affect the photocatalysis directly. The inertial components, such as NO, N_2O, or NO_3 molecules, would be adsorbed on the surface or enclosed in the mesopores of the particles, and not influence the electronic structure. The UV–vis spectra indicated that the visible activity came from the surface states, which was due to the NO binding to surface oxygen of TiO_2 without electronic transfer to the metal, which was also confirmed by EPR spectra. By comparison of the results of EPR and XPS, the higher activity of the catalyst derived from the mixture of ammonia and hydrazine hydrate was attributed the higher concentration of NO_2^{2-}, which depended on the nitrogen precursors. DFT calculations confirmed that the species of NO_2^{2-} can induce the formation of new energy levels near CB which is contributed to the visible light response of N-doped TiO_2 photocatalysts.

Acknowledgements

This work is sponsored by Scientific Research Foundation for the Returned Overseas China Scholars of MOE (2004527) and National Natural Science Foundation of China (NNSFC, 20636020). DFT calculations were supported by the Department of Materials & Engineering, Nanjing University. We would thank Dr. Qinghong Zhang (The State Key Laboratory of High Performance Ceramics and Superfine Microstructure, Shanghai Institute of Ceramics, Chinese Academy of Science) for his constructive suggestions and Dr. Yunxia Sui (Center of Modern Analysis, Nanjing University) for her helpful discussions about EPR.

References

[1] A. Fujishima, K. Honda, Nature 238 (1972) 37–38.
[2] M.R. Hoffmann, S.T. Martin, W. Choi, D.W. Bahnemann, Chem. Rev. 95 (1995) 69–96.
[3] Z. Zou, J. Ye, K. Sayama, H. Arakawa, Nature 414 (2001) 625–627.
[4] R. Asahi, T. Morikawa, T. Ohwaki, K. Aoki, Y. Taga, Science 293 (2001) 269–271.
[5] S. Sakthivel, H. Kisch, Angew. Chem. Int. Ed. 42 (2003) 4908–4911.
[6] W. Zhao, W. Ma, C. Chen, J. Zhao, Z. Shuai, J. Am. Chem. Soc. 126 (2004) 4782–4783.
[7] H. Sun, Y. Bai, Y. Cheng, W. Jin, N. Xu, Ind. Eng. Chem. Res. 45 (2006) 4971–4976.
[8] Y. Cheng, H. Sun, W. Jin, N. Xu, Chem. Eng. J. 128 (2007) 127–133.
[9] S. Sato, Chem. Phys. Lett. 123 (1986) 126–128.
[10] S.U.M. Khan, M. Al-Shahry, W.B. Ingler Jr., Science 297 (2002) 2243–2245.
[11] J.C. Yu, W. Ho, J. Yu, H. Yip, P.K. Wong, J. Zhao, Environ. Sci. Technol. 39 (2005) 1175–1179.
[12] J.C. Yu, J. Yu, Q. Ho, Z. Jiang, L. Zhang, Chem. Mater. 14 (2002) 3808–3816.
[13] X. Hong, Z. Wang, W. Cai, F. Lu, J. Zhang, Y. Yang, N. Ma, Y. Liu, Chem. Mater. 17 (2005) 1548–1552.
[14] T. Morikawa, R. Asahi, T. Ohwaki, K. Aoki, Y. Taga, Jpn. J. Appl. Phys. 40 (2001) L 561–L 563.
[15] H. Irie, Y. Watanabe, K. Hashimoto, J. Phys. Chem. B 107 (2003) 5483–5486.
[16] B. Kosowska, S. Mozia, A.W. Morawski, B. Grzmil, M. Janus, K. Kalucki, Solar Energy Mater. Solar Cells 88 (2005) 269–280.
[17] Y.C. Hong, C.U. Bang, D.H. Shin, H.S. Uhm, Chem. Phys. Lett. 413 (2005) 454–457.
[18] S. Sakthivel, H. Kisch, Chemphyschem 4 (2003) 487–490.
[19] D. Li, H. Haneda, S. Hishita, N. Ohashi, Mater. Sci. Eng. B 117 (2005) 67–75.
[20] S. Sakthivel, M. Janczarek, H. Kisch, J. Phys. Chem. B 108 (2004) 19384–19387.
[21] X.B. Chen, Y. Lou, A.C.S. Samia, C. Burda, J.L. Gole, Adv. Funct. Mater. 15 (2005) 41–49.
[22] Y. Nosaka, M. Matsushita, J. Nishino, A.Y. Nosaka, Sci. Technol. Adv. Mater. 6 (2005) 143–148.
[23] H. Sun, Y. Bai, W. Jin, N. Xu, Solar Energy Mater. Solar Cells 92 (2008) 76–83.
[24] M. Miyauchi, M. Takashio, H. Tobimatsu, Langmuir 20 (2004) 232–236.
[25] H. Kato, A. Kudo, J. Phys. Chem. B 106 (2002) 5029–5034.
[26] J.B. Yin, X.P. Zhao, Chem. Mater. 16 (2004) 321–328.
[27] T. Peng, H. Song, J. Xiao, H. Liu, J. Qin, J. Non-Cryst. Sol. 352 (2006) 3167–3174.

[28] T. Ihara, M. Miyoshi, Y. Iriyama, O. Matsumoto, S. Sugihara, Appl. Catal. B 42 (2003) 403–409.
[29] Y. Sakatani, J. Nunoshige, H. Ando, K. Okusako, H. Koike, T. Takata, J.N. Kondo, M. Hara, K. Domen, Chem. Lett. 32 (2003) 1156–1157.
[30] S. Joung, T. Amemiya, M. Murabayashi, K. Itoh, Appl. Catal. A 312 (2006) 20–26.
[31] S. Livraghi, M.C. Paganini, E. Giamello, A. Selloni, C.D. Valentin, G. Pacchioni, J. Am. Chem. Soc. 128 (2006) 15666–15671.
[32] Y. Li, D. Hwang, N.H. Lee, S.-J. Kim, Chem. Phys. Lett. 404 (2005) 25–29.
[33] S. Livraghi, A. Votta, M.C. Paganini, E. Giamello, Chem. Commun. (2005) 498–500.
[34] A. Hagfeld, Mi. Graetel, Chem. Rev. 95 (1995) 49–68.
[35] T. Lindgren, J.M. Mwabora, E. Avendano, J. Jonsson, A. Hoel, C. Granqvist, S. Lindquist, J. Phys. Chem. B 107 (2003) 5709–5716.
[36] Y.C. Chan, J.N. Chen, M.C. Lu, Chemosphere 45 (2001) 29–35.
[37] Z. Ai, P. Yang, X. Lu, J. Hazard. Mater. B 124 (2005) 147–152.
[38] K. Yang, Y. Dai, B. Huang, S. Han, J. Phys. Chem. B 110 (2006) 24011–24014.
[39] Z. Lin, A. Orlov, R.M. Lambert, M.C. Payne, J. Phys. Chem. B 109 (2005) 20948–20952.
[40] E. Finazzi, C.D. Valentin, A. Selloni, G. Pacchioni, J. Phys. Chem. C 111 (2007) 9275–9282.
[41] J. Graciani, L.J. Alvarez, J.A. Rodriguez, J.F. Sanz, J. Phys. Chem. C 112 (2008) 2624–2631.
[42] These calculations were accomplished by the DFT software package CASTEP, which is available from Accelrys, San Diego, CA. Geometry optimizations and energy calculations were performed using DFT within GGA, with the exchange-correlation functional of PBE. Energy cutoff was set to 340.0 eV and a $4 \times 4 \times 4$ *k*-point was adopted for calculations.
[43] J.Y. Lee, J. Park, J.H. Cho, Appl. Phys. Lett. 87 (2005), 011904-1-3.